Biomaterials 300 (2023) 122202

Contents lists available at ScienceDirect

Biomaterials

journal homepage: www.elsevier.com/locate/biomaterials

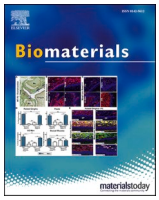

Liposome-anchored mesenchymal stem cells for radiation pneumonia/fibrosis treatment

Hailin Zhou [a], Yanxiang Zhang [a], Pei Pei [a], Wenhao Shen [a], Xuan Yi [b,**], Kai Yang [a,*]

[a] State Key Laboratory of Radiation Medicine and Protection, School of Radiation Medicine and Protection and School for Radiological and Interdisciplinary Sciences (RAD-X), Collaborative Innovation Center of Radiation Medicine of Jiangsu Higher Education Institutions, Soochow University, Suzhou, Jiangsu, 215123, China
[b] School of Pharmacy, Jiangsu Key Laboratory of Inflammation and Molecular Drug Targets, Nantong University, Nantong, Jiangsu, 226001, China

ARTICLE INFO

Keywords:
Mesenchymal stem cells
Radiation pneumonia/fibrosis
Anti-inflammatory immune
Click chemical reaction
Reactive oxygen species

ABSTRACT

The effectiveness of mesenchymal stem cells (MSCs) on inflammation-related disease is limited and the pharmaceutical preparation that was used to enhance the efficacy of MSCs cannot reach the diseased tissue in large quantities. Herein, antioxidant liposome (Lipo-OPC) is designed to anchor onto the surface of MSCs membrane via click chemical reaction (MSC-Lipo-OPC) without affecting the viability and physiological characteristics of MSCs, thus allowing efficient accumulation of MSC-Lipo-OPC in X-ray irradiated lung sites. More importantly, MSC-Lipo-OPC promotes the change of the quantity and polarity of innate immunocytes, mainly including neutrophils, macrophages and Tregs, in favor of anti-inflammatory, finally preventing the formation of radioactive pulmonary fibrosis. Therefore, it could enhance the treatment outcome of both of MSCs and drugs to radiation-induced lung injury via modifying the drug-loaded nanoparticle on the surface of MSCs membrane, further promoting the application of MSCs in radiation damage and protection.

1. Introduction

Exposure of the lung tissue to ionizing radiation at high dose, mainly during radiotherapy of thoracic tumors, can lead to the development of radiation pneumonia/pulmonary fibrosis [1]. In clinic, glucocorticoids and drugs with free radical scavenging capacity are common used to reduce the lung radiation injury and control respiratory symptoms [2]. However, the efficacy of these drugs is limited by their low pulmonary targeting, short retention time and inadequate anti-inflammatory efficiency [3]. Moreover, the current treatment is mainly symptomatic management and can cause certain side effects [4–6]. Therefore, there is an urgent need to develop an effective treatment strategy for reducing the severity of radiation pneumonitis and delaying the progression of radiation pulmonary fibrosis. At present, some radiation protection drugs or biomaterials have been explored to relieve radiation pneumonia/fibrosis [7,8]. The size-effect and inflammatory tendency characteristics are the main available strategies for targeting pneumonia [9,10]. Typically, micron-sized particles become lodged in the capillaries/fine bronchi of the lungs after intravenous or respiratory administration. In patients with chest tumors, especially elderly, there is often a series of underlying diseases leading to breathing difficulties, making intravenous administration more immediate and effective [11]. Once the drugs reach lung, they should fight inflammation and prevent pulmonary fibrosis by reducing reactive oxygen species (ROS) levels, activating the anti-inflammatory innate immunity and promoting tissue repair [12]. In this process, immune cells such as Tregs and macrophages as well as their secretion of cytokines play a major role [13,14].

Cell therapies have attracted widespread attention because of their targeting of diseases and certain therapeutic effect [15,16]. Mesenchymal stem cells (MSCs), as a typical representative, have been used in cancer treatment, tissue regeneration and anti-inflammatory therapy, due to their non-immunogenicity, immune modulating functions and anti-inflammatory/growth-promoting properties [17–19]. However, during the process of anti-inflammatory therapy, inflammatory environment with high ROS level can decrease the viability and pluripotency of the specifically targeting MSCs in the area of inflammation. Therefore, some drugs or biomaterials have been selected to cooperate with MSCs [20,21]. In situ acquisition of therapeutic proteins by genetic modification of MSCs is one approach, but this increases the risk of potential genotoxicity of MSCs [22]. Alternatively, MSCs can be directly administrated with chemical drugs via simultaneous injection, pre-incubation or cell surface modification [23,24]. Among them, drug-anchored cells

* Corresponding author.
** Corresponding author.
E-mail addresses: xuanyi@ntu.edu.cn (X. Yi), kyang@suda.edu.cn (K. Yang).

https://doi.org/10.1016/j.biomaterials.2023.122202
Received 14 March 2023; Received in revised form 1 June 2023; Accepted 7 June 2023
Available online 14 June 2023
0142-9612/© 2023 Elsevier Ltd. All rights reserved.

can be obtained by gently modifying the drug onto the cell surface via chemical reaction, such as click chemical reaction that is a fast, efficient, mild green chemical reaction [25,26]. In this way, the anchored drugs can act on both the inflammatory environment and MSCs post injection. Moreover, it can ensure the consistency of drugs and MSCs in time and space to maximize the synergistic effect.

In this study, oligomeric proanthocyanidin (OPC)-loaded liposome (Lipo-OPC) was linked to the membrane surface of MSCs with high joint efficiency via chick chemical reaction, obtaining drug-anchored MSCs (MSC-Lipo-OPC). This liposome was shown to have excellent free radical scavenging abilities, which could improve the function of MSCs and control the progression of inflammation. Upon intravenous injection of these MSCs, they could accumulate in large quantities in the X-ray-exposed lung tissue while not in healthy lung, owing to their characteristics of inflammatory tendency. In the early stages of lung damage, drug-anchored MSCs reduced the ROS production under the dual antioxidant repair of proanthocyanidins and MSCs. Notably, the number of infiltrating neutrophils, the main host cells producing ROS, was significantly reduced in X-ray-irradiated lung tissue after treatment with drug-anchored MSCs. Meanwhile, in the treated lung, macrophages could tend to be polarized towards M2, and a plenty of Tregs cells could infiltrate in lung tissue. These two kinds of innate immunocyte played an important role in the anti-inflammatory response through the production of various cytokines. Moreover, in the advanced stages of lung damage, drug-anchored MSCs could effectively relieve the severity of X-ray-induced lung fibrosis. Therefore, antioxidant liposome attached MSCs could regulate the function of innate immune cells in inflammation, reduce inflammatory response and delay the progression of pneumonia, providing an effective strategy for treating radiation pneumonia/fibrosis (Fig. 1).

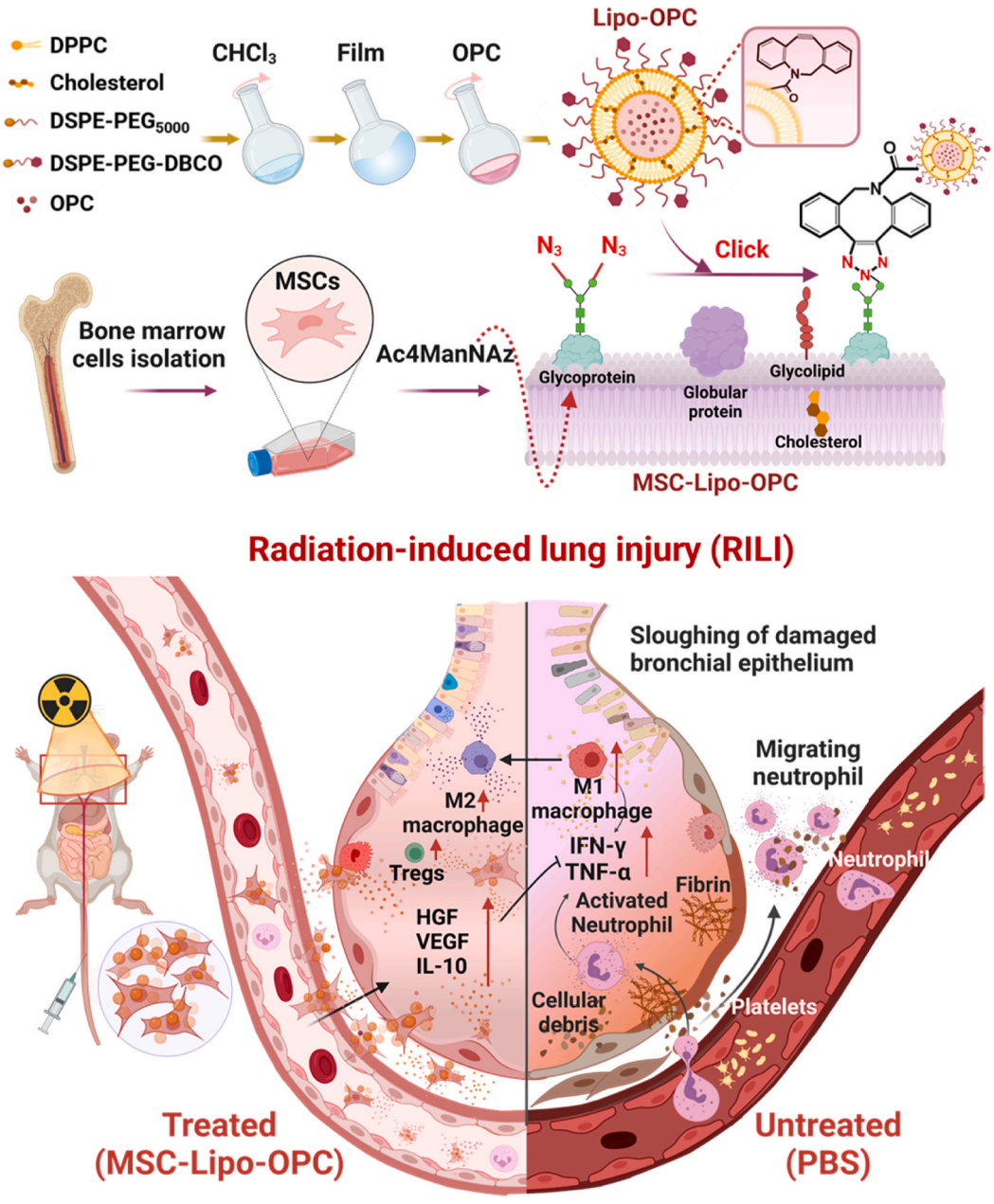

Fig. 1. The schematic illustration of MSC-Lipo-OPC-mediated radiation lung injury repair. DSPE-PEG-DBCO could be modified on OPC-loaded liposomes, and Ac4ManNAz could be exposed on the membrane surface of Ac4ManNAz-treated MSCs. MSC-Lipo-OPC was obtained through a click chemical reaction between DBCO-Lipo-OPC and Ac4ManNAz-treated MSCs. Moreover, MSC-Lipo-OPC targeted to the X-ray-exposed lungs and effectively relieved radiation pneumonia/fibrosis via regulating anti-inflammatory immune.

2. Materials and methods

2.1. Materials

1,2-dipalmitoyl-sn-glycero-3-phosphatidylcholine (DPPC), 1,2-distearoyl-sn-glycero-3-phosphoethanol-amine-N-(polyethylene glycol)-5000 (DSPE-PEG$_{5000}$), Cholesterol, dibenzocyclooctyl-modified DSPE–PEG (DSPE–PEG–DBCO) and Ac4ManNAz were purchased from Xi'an Ruixi Biological Technology Co., Ltd. (Xi'an, China). Oligomeric Proantho Cyanidin (OPC) was purchased from Shanghai Yuanye Biological Technology Co., Ltd. 2-(4-amidinophenyl)-6-indolecarbamidinedihydrochloride (DAPI) 1,1′-Dioctadecyl-3,3,3′,3′-Tetramethylindodicarbocyanine, 4-Chlorobenzenesulfonate Salt (DiD) and 1,1′-dioctadecyl-3,3,3′,3′-tetramethylindocarbocyanine perchlorate DiI) were acquired from Beyotime Technology. Matrix glue was obtained from Shanghai Nova Medical Technology Co., Ltd. The JC-10 assay kit was purchased from Beijing Solarbio Science & Technology Co., Ltd. (Beijing, China). Cell culture dishes/plates, round coverslips, 20-mm glass-bottom dishes, and centrifuge tubes were obtained from NEST Biotechnology Co., Ltd. (Wuxi, China). Malondialdehyde (MDA) assay kit and Superoxide Dismutase (SOD) assay kits were purchased from the Nanjing Jian cheng Bioengineering Institute (Nanjing, China). Mouse TNF-α ELISA Kit, Mouse IFN-γ ELISA Kit, Mouse HGF ELISA Kit and Mouse VEGF ELISA Kit were purchased from Multisciences (Lianke) Biotech Co., Ltd. (Zhejiang, China). Myeloperoxidase Rabbit mAb and vimentin Rabbit mAb were purchased from Zen BioScience Co., Ltd. (Wuhan China).

2.2. The collection of MSCs

Three-week-old male C57BL/6 J mice were purchased from GemPharmatech Co., Ltd. (Jiangsu, China), and were used to collect their bone marrow mesenchymal stem cells. C57BL/6 J mice aged 6–8 weeks were purchased for other animal experiments. All of mice in this study were raised under specific pathogen-free conditions and animal-related treatments were performed in accordance with procedures and protocols approved by the Animal Care and Welfare Committee of the Animal Center of Soochow University.

Mouse bone marrow mesenchymal stem cells (mBMSCs) were isolated and cultured as reported previously [27]. Briefly, the bone marrow cells were flushed out from mouse femurs and tibias with 5% heat-inactivated FBS in DMEM/F12 -Dulbecco's Modified Eagle Medium. All nucleated cells were seeded on 100 mm culture dishes (Corning, USA) at 37 °C in 5% CO_2. Non-adherent cells were removed after 72 h and attached cells were cultured for 7 days in DMEM/F12 supplemented with 10% FBS, 2 mM of L-glutamine, 55 μM of 2-mercaptoethanol (Invitrogen, USA), 100 U/ml of penicillin and 100 μg/mL of streptomycin.

2.3. Preparation and characterization of Lipo-OPC NPs

The preparation of Lipo-OPC was divided into two steps, low pressure rotary steaming and thin layer emulsification. Firstly, DPPC, DSPE-PEG5000, cholesterol, DSPE-PEG-DBCO were weighed in proportion (22:12:8:3), dissolved with trichloromethane, and added to the round-bottomed flask. The trichloromethane was removed by vacuum and low pressure gyroevaporator (temperature parameter: 45 °C), and a lipo-film was formed at the bottom of the round-bottomed flask. Next, the lipo-film was emulsified into nanoparticles, and OPC aqueous solution was added to the bottom of the bottle at 40 °C. After 1 h of ultrasound, the lipo-film was repeatedly extruded 5 times by a 200 nm liposome extruder. Finally, the free drugs were removed by centrifugation through an Amico filter device (MWCO = 100 kDa) and washed with PBS. The hydrodynamic diameter, polydispersion index (PDI) and surface charge (zeta potential) of the nanoparticles was determined by dynamic laser scattering (Malvern, Zetasizer Nano ZS90, United Kingdom).

2.4. The antioxidant property of Lipo-OPC

Firstly, the cytotoxicity of Lipo-OPC was tested. MSCs, mouse alveolar epithelial cells (MLE-12) and human umbilical vein endothelial cell (HUVEC) were planted in 96-well plates at the cell density of 8000/well. Then Lipo-OPC was added at different concentrations (3.9 7.8 15.6 31.3 62.5125.0 μg/mL of OPC). 24 h later, cell counting kit-8 (CCK-8) reagent (Solarbio, Beijing, China) was added and incubated for 2–4 h. The absorption value at 450 nm was measured by microplate reader.

In order to check the antioxidant property of Lipo-OPC, mouse alveolar epithelial cells (MLE-12) were planted on six-well plates (15×10^4 per well) and irradiated by X-ray at the dose of 10 Gy. OPC-loaded liposome or naked liposome was added after the X-ray exposure. 24 h later, the ROS probe H2DCFHDA (5 μM) was added to the dish and incubated with cells in the dark for 1 h. Finally, the ROS content of the digestive cells was analyzed by flow cytometry (BD FACSVerse, USA). HUVEC, MLE-12 cells and BEAS-2B cells were cultured on confocal dishes. After the cells were treated by X-ray and Lipo-OPC, the superoxide anion probe was added to the confocal dish and incubated with the cells for 10 min, and the intensity of the red fluorescence signal of Dihydroethidium (DHE) was observed under a confocal microscope.

Finally, the decreased mitochondrial membrane potential was measured by JC-10 assay (Solarbio, Beijing, China). MLE-12 cells were cultured overnight on a six-well plate (15×10^4 per well). After 24 h treatment with X-ray and Lipo-OPC, 1 mL of JC-10 ($1 \times$) solution of mitochondrial membrane potential reagent was added to the Petri dish at 37 °C for 20 min. The contents of JC-10 monomer (FITC-green) and JC-10 polymer (PI-red) were analyzed by flow cytometry.

2.5. The preparation of lipo-OPC-anchored MSCs Lipo-OPC-anchored MSCs

In order to prepare MSC-Lipo-OPC, 1×10^6 MSCs cells inoculated into 100 mm plate with DMEM/F12 medium containing 10 μM Ac4ManNAz at 37 °C and 5% CO_2 incubator for 48 h. Then, medium was removed and the cells were wished three times with PBS. Next, serum-free medium with Lipo-OPC (OPC = 30 μg/mL) was added and incubated for 1 h at 37 °C. The cells were washed twice with PBS and collected after trypsin digestion. The cell suspension was centrifuged at 1000 rpm for 5 min. The final precipitated MSC-Lipo-OPC was re-suspended in PBS for further study. Conjunction between MSC and Lipo-OPC was imaged by CLSM (FV1200, OLYMPUS) and the cold field emission high resolution scanning electron microscope (S-4700, Hitachi.)

To check the cytotoxicity of this treatment for MSCs, DMEM/F12 medium containing 10 μM of Ac4ManNAz and 30 μg/mL of Lipo-OPC were incubated with MSCs. The CCK-8 assay was performed at 24 h and apoptosis analysis was measured at 48 h using apoptosis kit. Cell cloning experiments were performed on 6 well plates with 400 MSCs treated with different reagents per well. One week later, the dye was stained with crystal violet for 30 min, and the photos were taken after washing with PBS.

2.6. Effect of Lipo-OPC modification on the feature of MSCs

The migration ability of MSC-Lipo-OPC was investigated by transwell cell migration assay. The experiment was divided into three groups: CXCL 12 (−) plus MSC, CXCL 12 (+) plus MSC and CXCL 12 (+) plus MSC-Lipo-OPC. Firstly, 2×10^4 MSC or MSC-Lipo-OPC were cultured in the transwell insert for 24 h. DMEM/F12 and CXCL12 (15 μg/mL) containing 10% fetal bovine serum were added to transwell lower chamber. After 48 h, the chamber was stained with crystal violet and the excess dye was washed away. The crystal violet solid was dissolved with 33% glacial acetic acid for measuring the absorbance of the solution at 570 nm.

To investigate the ability of MSC-Lipo-OPC to promote vascular endothelial cell growth, we conducted transwell angiogenesis assay. A

mixture of 30 μL matrix glue and 30 μL DMEM/F12 was pre-laid on the bottom of the lower chamber plate of 24-well transwell. MSCs and MSC-Lipo-OPC were inoculated in the upper chamber and incubated for 24 h at 37 °C and 5% CO_2. In the second step, 30,000 HUVECs were inoculated into the lower compartment. The upper layer of paracrine factors fed the lower layer of HUVEC, and the angiogenic culture lasted for 8 h. The angiogenesis analysis software in image J was used for analysis.

2.7. Fluorescent imaging

Healthy mice and mice with RILI were intravenously injected with Lipo-OPC and MSC-Lipo-OPC, and then imaged by IVIS imaging system (PerkinElme) at different time points (2, 5, 12, and 24 h). Mice were euthanized after the last time-point imaging, lungs and other main organs were harvested for ex vivo imaging, and fluorescence ROI was calculated.

2.8. The treatment effect of MSC-Lipo-OPC on radiation pneumonia

The healthy mice were randomly divided into 6 groups, a: control group (Health), b: radiation lung injury group (IR + PBS), c: Lipo-OPC injection group (IR + Lipo-OPC), d: MSC injection group (IR + MSC), e: positive radiation protector group (IR + Amifostine), and f: MSC-Lipo-OPC injection group (IR + MSC-Lipo-OPC). To establish the radiation-induced lung injury model, mice were anesthetized and their whole chest was exposed to a single dose of 15 Gy X-ray (X-RAD320ix, 320 kV, 2 Gy/min, PXi, USA). During the irradiation, the other body parts were placed with shielding lead plates. The survival state and body weight of mice in each group was monitored within 30 days. Amifostine were intraperitoneally injected at the dose of 0.3 mg/kg at 30 min before X-ray exposure. MSC or MSC-Lipo-OPC was injected intravenously at the dose of 3×10^6 within 1 h after X-ray exposure.

The serum and lungs were collected from mice with different treatments at appointed time. The contents of TNF-α, IFN-γ, HGF, VEGF and other cytokines in serum were determined by enzyme-linked immunosorbent assay (ELISA). The contents of MDA and SOD in lungs were detected by biochemical kit (Nanjing Jiancheng Bioengineering Institute, Nanjing, China). The lung sections (10 μm) were obtained and investigated by H&E, Masson, and immunofluorescence (IF) staining. The levels of MPO and vimentin were evaluated by IF analysis (Myeloperoxidase Rabbit mAb: Art-No-R25062 and vimentin Rabbit mAb: Art-No-R22775).

2.9. Flow cytometric analysis of neutrophils

After the lung tissue was digested by tissue digestion enzymes (Hyaluronidase, Collagenase IV, Collagenase I), cells were obtained through 200 meshes nylon sieve and filtered/washed twice at 1xFACS (4 °C, 654 g for 5 min). Then, the Cells (5×10^7/mL) were re-suspended with 1 mL 40% Percoll, and stratified after centrifugation (4 °C, 805 g for 30 min). The first layer of fluid containing macrophages and lymphocytes was aspirated, and neutrophils in the second layer were collected. CD45-PE-Cy7 (eBioscience™, clone: 30-F11, 25-0451-82), Ly6G-FITC (eBioscience™, clone: 1A8-Ly6g, 11-9668-82) and CD11B-PE (eBioscience™, clone: M1/70, 12-0112-82) were added in sequence, incubated at 4 °C for 1 h, washed and suspended by FACS. Finally, neutrophils were detected and analyzed by flow cytometry.

2.10. Flow cytometric analysis of macrophages

Cell suspension was prepared according to the method described above, and cells were then labeled by anti-mouse F4/80-FITC antibody (Catalog No. E-AB-F0995C), anti-mouse CD11b-PerCP antibody (Catalog No. E-AB-F1081F), PE CD86 monoclonal antibody (Catalog No. GL1) and anti-mouse CD206-APC antibody (Catalog No. MR6F3). In order to be labeled by anti-CD206-APC antibody, the cells were firstly fixed with fixation buffer (420,801, BioLegend) for 30 min at room temperature. Then, fixative was removed, and 1 × Intracellular Staining Permeabilization Wash Buffer (421,002, BioLegend) was added to break the nuclear membrane for 1 h. Anti-CD206-APC antibody stained the cells in a permeable fluid. Finally, the free dye was washed and the fluorescence signal of macrophage-labeled antibody was detected by flow cytometry.

2.11. Flow cytometric analysis of tregs Tregs

Cell suspensions were labeled with anti-mouse CD3-FITC (eBioscience™, clone: 17A2, 11-0032-82) and anti-mouse CD4-APC (eBioscience™, clone: GK1.5, 17-0041-83) by surface staining. Cell fixation and nuclear membrane breaking were performed using Foxp3/Transcription Factor Staining Buffer Set (eBioscience™, 00-5523-00). Finally, intracellular Foxp3 staining was performed using anti-mouse Foxp3-PE (eBioscience™, clone: NRRF-30, 72-5775-40).

2.12. Lung function test and CT imaging

In order to test the lung function of mice with different treatments, sensors (STARR Life Sciences ®, Oakmont, PA) were clamped to the necks of mice and let them move freely in their cage. The sensor-linked software MouseOx Plus monitored the mice's heart rate, respiratory rate, oxygen saturation and pulse expansion. Besides, the U-SPECT+/CT imaging system for small animals (MILabs, Utrecht, the Netherlands) was used to image the pulmonary fibrosis of mice.

2.13. Statistical analysis

All data were expressed as mean ± SD/SEM. Student's *t*-test (two-tailed) or one-way analysis of variance (ANOVA) was performed in this study. All statistical analyses were performed using GraphPad Prism 7.00 (GraphPad Software Inc. USA). The probability values less than 0.05 were considered statistically significant. The detailed statistical analysis description was showed in each figure caption.

3. Results and discussion

3.1. Preparation and antioxidant property of Lipo-OPC

In order to obtain biomaterials with antioxidant ability, we selected liposome to load OPC. The characteristics of prepared Lipo-OPC and its ROS scavenging ability had been tested. Like to various liposomes, Lipo-OPC showed a spherical vesicle structure with the size of about 100 nm in transmission electron microscopy (TEM) images (Fig. 2A). Compared with naked liposomes, Lipo-OPC showed slightly bigger size in TEM image (Fig. S1) Similarly, the hydration radius of Lipo-OPC was about 60–200 nm, which was bigger than that of the naked liposome, and its PDI value was between 0.1 and 0.3, indicating that it had good stability (Fig. 2B). Meanwhile, the surface negative zeta potential of liposomes increased when being loaded with OPC, probably owing to the certain lipophilicity of OPC, leading to enhanced colloidal stability and reduced cell uptake of Lipo-OPC (Fig. 2C). Next, ultraviolet–visible (Uv–Vis) and fourier transform infrared spectroscopy (FTIR) were performed on OPC, naked liposome and Lipo-OPC to verify the existence of OPC in Lipo-OPC. From the results in Fig. 2D&E, Lipo-OPC showed the characteristic absorption peak of OPC in both Uv–Vis and FTIR spectrum. After calculation, the loading rate of OPC was 20.12% ± 0.92%, and its encapsulation rate was 97.01% ± 1.18%. Additionally, the hydrophobic layer of Lipo-OPC could also be loaded with DiD dye, which was convenient to observe the traces of Lipo-OPC in animal experiment. Furthermore, we also tested the bioactivity of Lip-OPC. Firstly, the cytotoxicity tests were carried out on different cells including human umbilical vein endothelial cells (HUVEC), murine lung epithelial-12 cells (MLE-12) and MSCs. The results showed that 31.3 μg/mL of Lipo-OPC had limited cytotoxicity to the tested cells, and 15.6 μg/mL of

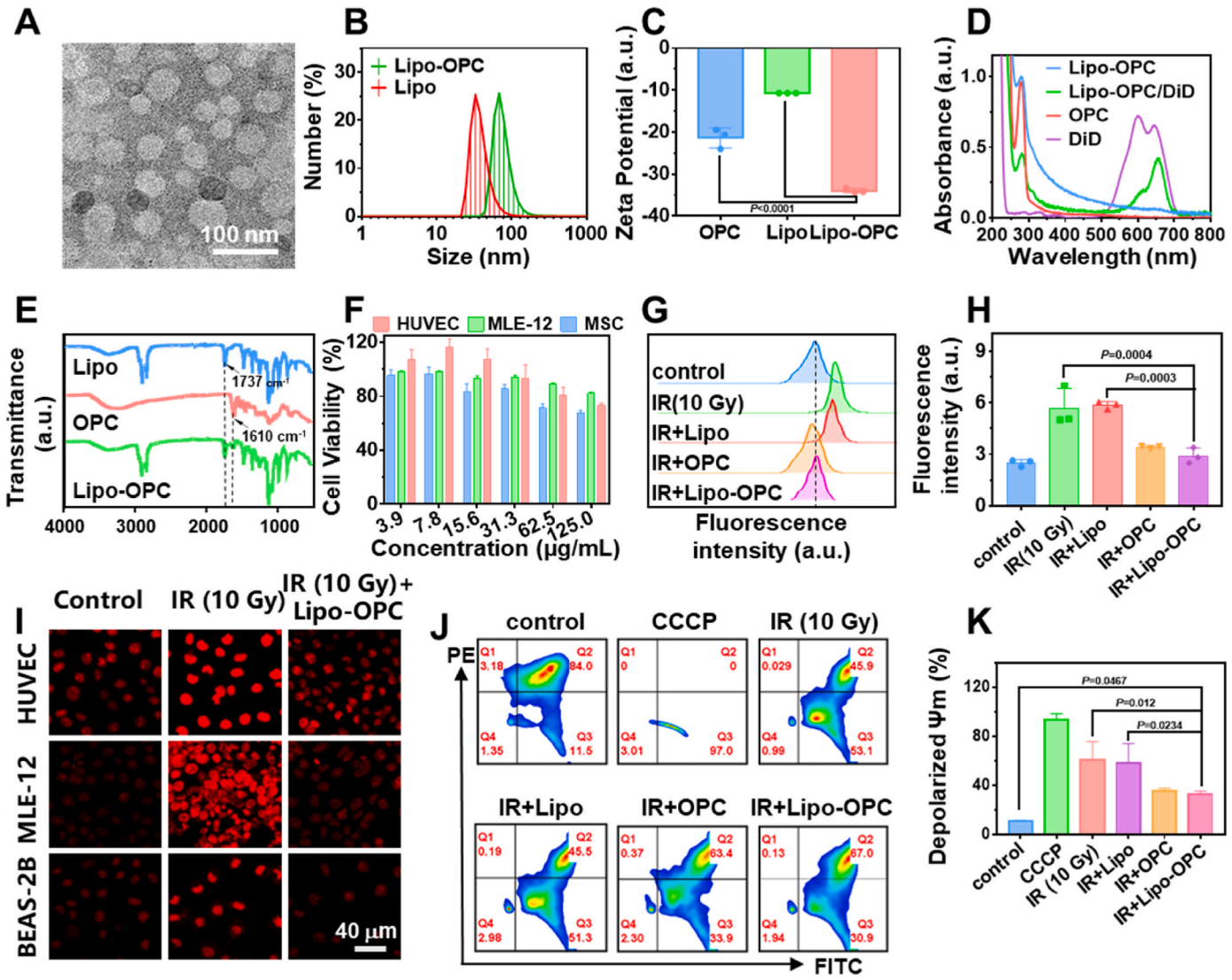

Fig. 2. The preparation and ROS scavenging capacity of Lipo-OPC. (A)The TEM image of Lipo-OPC nanoparticles negatively stained with phosphotungstic acid. (B) The hydration radius of Lipo-OPC and naked liposome. (C) The Zeta potential of free OPC, Liposome and Lipo-OPC. (D) The UV absorption spectrum of OPC, DiD, Lipo-OPC and Lipo-OPC-DiD. (E) Fourier infrared spectrum of Liposome, OPC and Lipo-OPC. (F) The cell viability of MSC, MLE-12 and HUVEC cells after incubation with Lipo-OPC for 24 h. (G, H) The representative flow diagram (G) and statistical data (H) of ROS fluorescence in cells with various treatments (n = 3). (I) The confocal images of superoxide anions in HUVEC, MLE-12 and BEAS-2B cells with indicated treatments. The red fluorescence intensity was positively proportional to the concentration of superoxide anions. (J, K) The mitochondrial membrane potential of cells with different treatments measured by flow cytometry using a JC-10 probe (n = 3). Carbonyl cyanide 3-chlorophenylhydrazone (CCCP) indicated the positive control to induce mitochondrial destruction. Statistical significance was calculated via one-way analysis of variance (ANOVA).

Lipo-OPC could promote the proliferation of HUVEC by 7%–16%, reflecting that the low concentration of OPC could promote cardiovascular regeneration (Fig. 2F). Secondly, the damage of ionizing radiation to human body is mainly through inducing the mass production of ROS, while OPC has been reported to clear ROS effectively [28–30]. To assess the ability of Lipo-OPC to scavenge oxygen radicals in X-ray-exposed cells, intracellular singlet oxygen concentration was detected by flow cytometry using an ROS probe (H2DCFH-DA). Lipo-OPC significantly reduced the X-ray-triggered ROS level in cells but naked liposome could not, suggesting that Lipo-OPC was an effective radioprotectant (Fig. 2G&H). Among the various types of ROS, superoxide anions ($O_2^{\cdot-}$) are closely associated with many inflammatory diseases [31,32]. Lipo-OPC could significantly reduce the concentration of superoxide anions in three types of cells associated with lung injury (Fig. 2I). Finally, the effect of Lipo-OPC on radiation-induced mitochondrial membrane potential (Δψm) was also investigated by flow cytometry using JC-10 dye. Radiation exposure resulted in a significant reduction in mitochondrial membrane potential, while Lipo-OPC could reduce the radiation-induced loss of mitochondrial membrane potential by 20%, further reducing the mitochondrial membrane penetration and membrane potential decomposition, and preventing early apoptosis or necrosis of cells (Fig. 2J&K).

3.2. *The construction and the characters of MSC-Lipo-OPC*

Next, Lipo-OPC nanoparticle had been anchored onto the surface of MSCs membrane via click chemical reaction. The MSCs were extracted from bone marrow of C57BL/6 mice according to the standard protocol [27] and observed under a microscope in a fusiform or star shape (Fig. S2). Consistent with international society for cell therapy (ISCT) standards [33], we found that bone marrow mesenchymal stem cells (BMSCs) highly expressed CD105 and CD90, but CD45 was negatively expressed (Fig. S3). Currently, metabolic sugar engineering is often used to deliver specific chemical groups into cells, and

N-azidoacetylmannosamine-tetraacylated (Ac4ManNAz) is the building block of sialic acid, which is the most abundant glycan on the surface of cells [34,35]. During cell metabolism, Ac4ManNAz is used to synthesize sialic acid and the azide groups would be exposed on the cell surface. The alkyne group of DBCO could easily react with the azide group in the absence of copper [36]. Therefore, DSPE-PEG-DBCO-modified Lipo-OPC could be linked to Ac4ManNAz-treated MSCs at 37 °C for 1 h (Fig. 3A). Moreover, this treatment could not affect the cell viability, owing to the required low concentration of Ac4ManNAz (10 μM) and Lipo-OPC (30 μg/mL of OPC) (Fig. 3B). Besides, Ac4ManNAz and Lipo-OPC induced very little apoptosis to MSCs, and the colony forming ability of MSCs, Ac4ManNAz-treated MSCs and MSC-Lipo-OPC-treated MSCs were almost the same (Fig. 3C and D&S4).

Furthermore, the localization of Lipo-OPC on the membrane surface of MSCs was determined by confocal laser scanning microscopy (CLSM) and scanning electron microscopy (SEM). MSCs without Ac4ManNAz could only uptake a small number of Lipo-OPC into the cytoplasm, while a plenty of Lipo-OPC could anchored to the membrane surface of Ac4ManNAz-treated MSCs (Fig. 3E). Similarly, SEM images exhibited some small nanoparticles on the surface of Ac4ManNAz-treated MSCs, further indicating the successful modification of Lipo-OPC on MSCs (Fig. 3F). Additionally, we adopted flow cytometry and confocal microscopy to detect the endocytosis of Lipo-OPC by MSCs during the preparation and incubation of MSC-Lipo-OPC. Ac4ManNAz-treated MSCs were incubated with Lipo-OPC (without DBCO) (MSCs + Lipo-OPC) or Lipo-OPC (with DBCO) (MSC-Lipo-OPC) for 1 h, respectively. The DiD intensity of MSC + Lipo-OPC reflected the endocytosis plus adhesion of Lipo-OPC in the preparation of MSC-Lipo-OPC, and the DiD intensity of MSC-Lipo-OPC indicated the total Lipo-OPC of MSC-Lipo-OPC. The results showed that less than 39.92% ± 1.39% of the total Lipo-OPC of MSC-Lipo-OPC was endocytosed by MSCs (Fig. S5). Besides, most of the anchored Lipo-OPC nanoparticles on the membrane surface of MSCs could remain on the membrane in 8 h, and some of them were gradually internalized into the cells in 24 h (Fig. S6). More importantly, Lipo-OPC modification could not affect the nature of MSCs, such as inflammatory tendency and angiogenesis promotion. Both of MSCs and MSC-Lipo-OPC could migrate to the high concentrations of CXCL12 chemokine (15 μg/mL) in transwell invasion assay, reflecting that chemokine receptors on stem cell surface were not occupied and inflammatory tendency of MSCs was retained for MSC-Lipo-OPC (Fig. 3G&H). In addition, the angiogenic activity of MSC-Lipo-OPC was then examined. MSCs and MSC-Lipo-OPC were inoculated in the upper chamber of transwell 48 h in advance, and HUVECs were then inoculated into the substrate-coated underside. HUVECs were adherent to the wall for 8 h in the nutrient supply of the upper compartment cell secretory factor, resulting in the angiogenesis (Fig. 3I). The cell images and their quantitative analysis showed that the total vessel length, the number of nodes and junctions, and the number of branches per field of view in the MSC-Lipo-OPC group were higher than those in the control group, suggesting the same paracrine activity between MSCs and MSC-Lipo-OPC for early vascular repair and reconstruction (Fig. 3J-M&S7). Besides, MSC-Lipo-OPC secreted much more IL-10, VEGF and HGF than the initial MSCs, suggesting that Lipo-OPC modification enhanced the anti-inflammatory (IL-10), pro-angiogenesis (VEGF) and pro-repair (HGF) abilities of MSCs (Fig. S8). Notably, Lipo-OPC-endocytosed MSCs showed almost the same potency as MSCs, indicating that the low endocytosis of Lipo-OPC in the preparation and incubation process could not affect the potency of MSCs.

3.3. The targeted delivery of MSC-Lipo-OPC to RILI site

Next, we wanted to investigate whether MSC-Lipo-OPC could relieve the radiation-induced lung injury (RILI). The targeting delivery of MSC-Lipo-OPC to X-ray-exposed lung was the prerequisite for its effectiveness. Therefore, utilizing its micron size and inflammatory tendency, MSCs were intravenously injected into healthy mice or mice with RILI to test the targeting ability of MSCs to X-ray-exposed lung. After intravenous administration, DiD labeled MSCs was slightly enriched in the lungs of healthy mice, but accumulated significantly at the site of RILI (Fig. 4A&B). After fluorescence quantification, the accumulation in RILI site at 12 h was about 1.5 times that of healthy lung, indicating that the enhanced lung accumulation of MSCs could be realized after X-ray exposure to the lungs. We then examined the pulmonary residency of MSC-Lipo-OPC/DiD and Lipo-OPC/DiD in healthy mice and RILI mice. The DiD was loaded by Lipo-OPC and its signal in mice reflected the distribution of Lipo-OPC. In healthy mice, MSC-Lipo-OPC did not accumulate for a long time because the lungs did not have inflammation. Moreover, for mice with RILI, the retention time of MSC-Lipo-OPC in the inflammation site was longer than that of Lipo-OPC (Fig. 4C&D). The accumulation of MSC-Lipo-OPC in the lungs at 24 h was 2.73 times that of Lipo-OPC, and 5.27 times that of MSC-Lipo-OPC in healthy lungs (Fig. 4E&F). Similarly, the confocal images of lungs collected from the above three groups showed that the strongest DiD fluorescence in the extensive interstitial interior of the lung could be found in MSC-Lipo-OPC-treated RILI lung (Fig. S9). All of these results proved the perfect targeting ability of MSC and its loaded Lipo-OPC to lung inflammation.

3.4. MSC-Lipo-OPC for relieving radiation pneumonia

Motivated by the targeted delivery of MSC-Lipo-OPC to X-ray-exposed lung, the radiation protection of MSC-Lipo-OPC for RILI was then explored. Healthy C57BL/6 mice weighing 19–21 g were anesthetized and given a single dose (15 Gy) of chest irradiation. MSCs or MSC-Lipo-OPC was intravenously injected at 3 h, 7 d, 14 d and 30 d after X-ray exposure (Fig. 5A). The body weight of all mice was recorded in 30 days after X-ray exposure and used for preliminary evaluation of the therapeutic effect of MSC-Lipo-OPC on RILI. Severe weight loss was observed on the third and ninth days after radiation, when the hematopoietic system in the mice was first damaged. After 10 days, the mice in each group gained weight slowly. However, the upward trend of ionizing radiation (IR) + PBS-treated group was much lower than that of the other four groups (Fig. 5B). Visually, various degrees of skin damage and hair loss in the irradiated field of the chest of mice were found in the irradiated group. Transplantation of MSCs and MSC-Lipo-OPC could reduce the severity of hair abnormalities and skin lesions (Fig. 5C). Meanwhile, from the hematoxylin-eosin (H&E) staining images, we could find hyperemia, bleeding and lymphocytes/plasma cells infiltration in tissue interspace and alveolar cavity in X-ray-treated lung at 33 days after irradiation, which were the specific histopathological features of RILI. In this pathological process, the alveolar septal fibroblasts could proliferate to form a dense transparent membrane, and the respiratory air cavity shrinks to a fissure. All of MSCs, Lipo-OPC and MSC-Lipo-OPC could significantly reduce pneumonia and the effect of MSC-Lipo-OPC was the best. Compared with PBS, MSC-Lipo-OPC had the ability to maintain normal lung tissue morphology (Fig. 5D). Additionally, no significant hepatorenal pathological changes were observed in mice, indicating that the material had no obvious toxic effects on the treated mice (Fig. S10).

Malondialdehyde (MDA) level is a key indicator of oxidative stress and superoxide dismutase (SOD) is closely related to the clearance of ROS. Therefore, the MDA and SOD level in each group were tested. As showed in Fig. 5E, the MDA level was reduced 4 times after MSC-Lipo-OPC treatment for X-ray-exposed mice. On the contrast, the SOD level in the MSC-Lipo-OPC-treated mice was 2.5 times higher than that in the RT + PBS-treated mice (Fig. 5F). The variation trend of these two indicators reflected that MSC-Lipo-OPC could promote the clearance of ROS and then decrease the severity of inflammation. In the inflammatory region, neutrophils could generate a plenty of ROS via myeloperoxidase (MPO) to eliminate the invading pathogens [7]. Thus, the number of neutrophil immune cells extracted from the lung tissue was counted by flow cytometry, following the gated strategy of $CD45^{+}Ly6G^{+}CD11b^{+}$ (Fig. 5G&H). The number of neutrophils increased significantly to 42.1% after irradiation, and MSC-Lipo-OPC

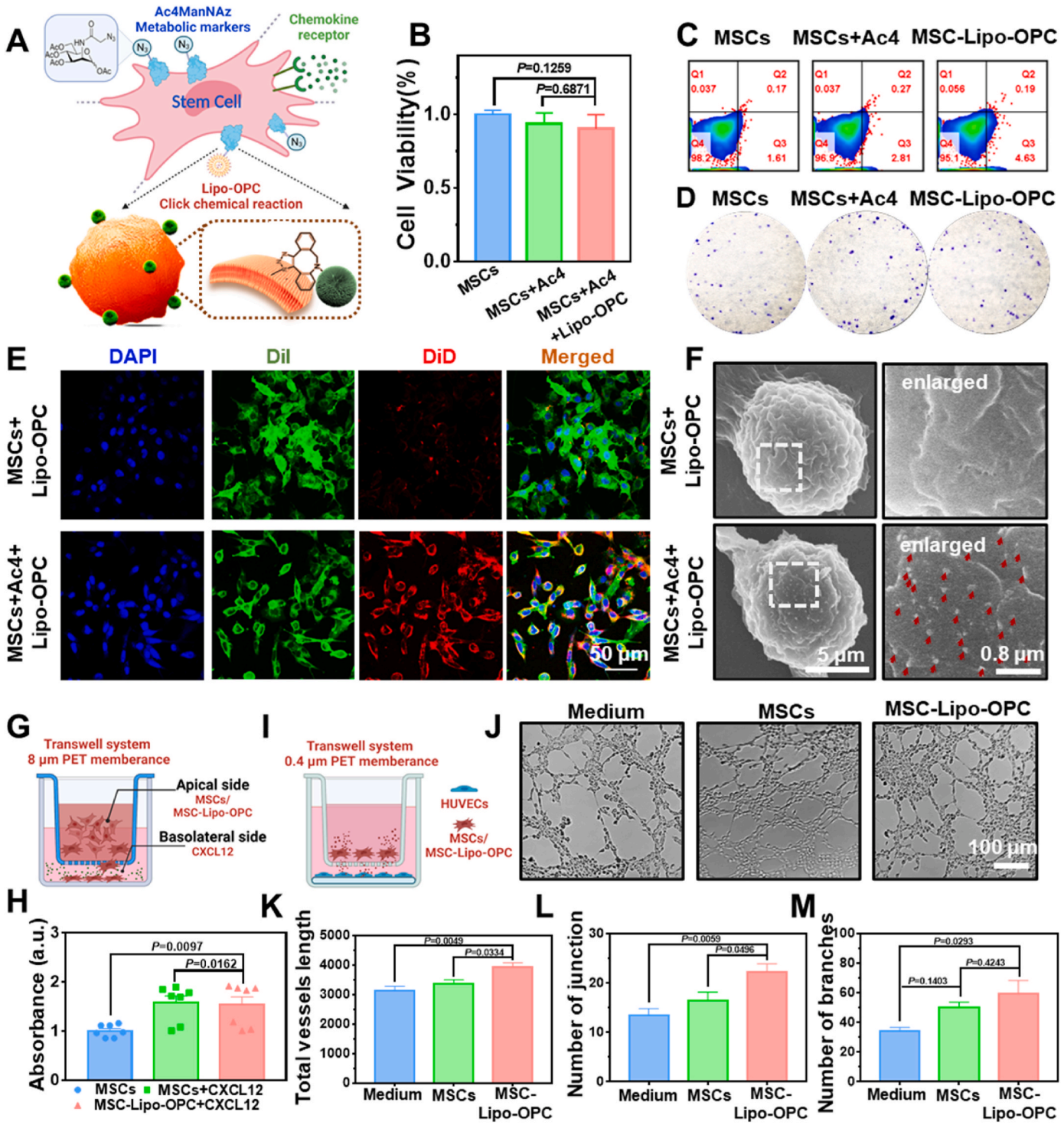

Fig. 3. The preparation of MSC-Lipo-OPC and the effect of Lipo-OPC modification on the viability and properties of MSCs. (A) The schematic diagram showing the structure of MSC-Lipo-OPC. DBCO of Lipo-OPC could mediate the link of Lipo-OPC and Ac4ManNAz-treated MSCs. (B) Relative cell viability of MSCs after incubation with Ac4ManNAz and Lipo-OPC for 24 h (n = 3). (C) Representative flow diagrams of apoptosis of MSCs, MSCs incubated with Ac4ManNAz for 48 h (MSCs + Ac4) and MSCs incubated with Ac4ManNAz for 48 h and then Lipo-OPC for 1 h (MSC-Lipo-OPC). (D) Representative photographs of cell clonal communities formed from MSCs, MSCs + Ac4 and MSC-Lipo-OPC after one week. (E) The confocal images of MSCs treated with Lipo-OPC and MSCs treated with both of Ac4ManNAz and Lipo-OPC. DAPI (blue) indicated to cell nucleus, DiI (green) indicated to cell membrane of MSCs and DiD (red) indicated to Lipo-OPC-DiD. (F) SEM images of MSC and MSC-Lipo-OPC. Red arrow showed the nanoparticles on the membrane surface of MSCs. (G–H) The migration ability of MSCs and MSC-Lipo-OPC in an environment with high concentration of CXCL12 (n = 7). (I–M) The representative images (J) and statistical data (K–M) showing the angiogenesis promotion of MSCs and MSC-Lipo-OPC (n = 4). Scale bar = 100 μm. Statistical significance was calculated via one-way analysis of variance (ANOVA).

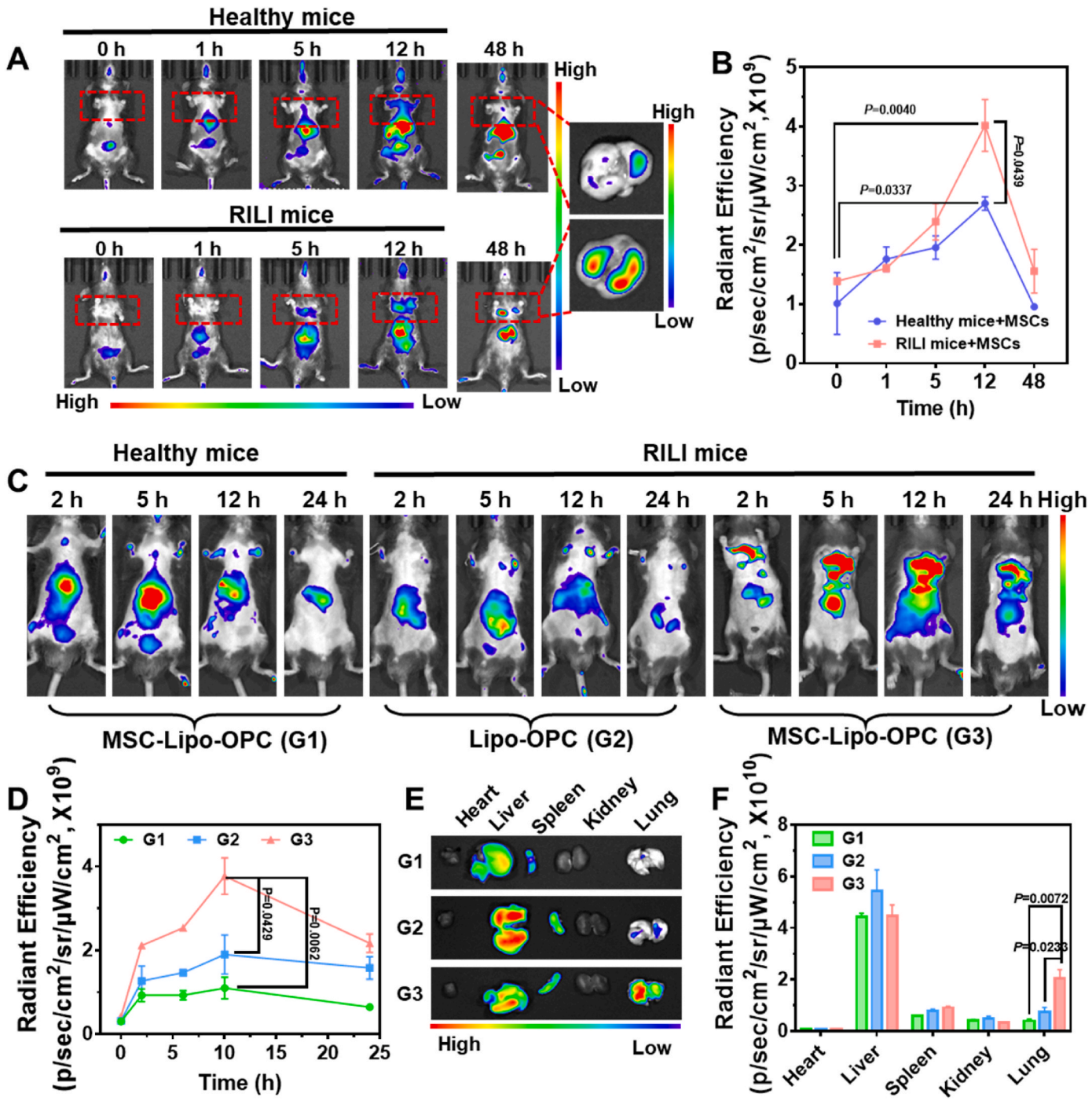

Fig. 4. The targeted delivery of MSC-Lipo-OPC to X-ray-exposed lungs. (A) In vivo fluorescence images and fluorescence signal values (B) of healthy mice and RILI mice intravenously injected with DiD-MSCs (n = 3). (C) Fluorescence imaging of healthy mice injected with MSC-Lipo-OPC-DiD (G1), RILI mice injected with Lipo-OPC-DiD (G2) and RILI mice injected with MSC-Lipo-OPC-DiD (G3). (D) Fluorescence quantification of the mice chest in C (n = 3). (E, F) The main organs collected from mice in G1, G2 and G3 were imaged (E) and quantified (F) (n = 3). T-tests were used for compare means between groups.

treatment significantly reduced the inflow of neutrophils to 17.37%, which was more similar to the number of neutrophils in the healthy lung. This level of neutrophils could maintain innate immunity in lung and not induce extra ROS to destroy lung tissue. Furthermore, pulmonary MPO was identified by immunofluorescence to indicate the extent of neutrophil activation in lung tissue. As shown in Fig. 5I&J, MSC-Lipo-OPC significantly reduced the activation and accumulation of neutrophils in the lung, thereby inhibiting the production of excessive oxidants by MPO and reducing the recurrence of oxidative tissue damage.

3.5. Anti-inflammatory immune regulation of MSC-Lipo-OPC

In addition to neutrophils, other innate immune cells, mainly including macrophages and regulatory T cells, are also involved in the inflammatory process, while M2 and Treg are benefit to fight inflammation. To analyze the effect of MSC-Lipo-OPC on the polarization of macrophages in RILI, macrophage markers (F4/80 and CD11b) in the lung tissue were identified by flow cytometry (FACS). The representative FACS diagram showed the different gating strategies of macrophages' two subpopulations, F4/80^{hi}CD11b^{+} CD86^{+} pro-inflammatory macrophages (M1, M1 subtype

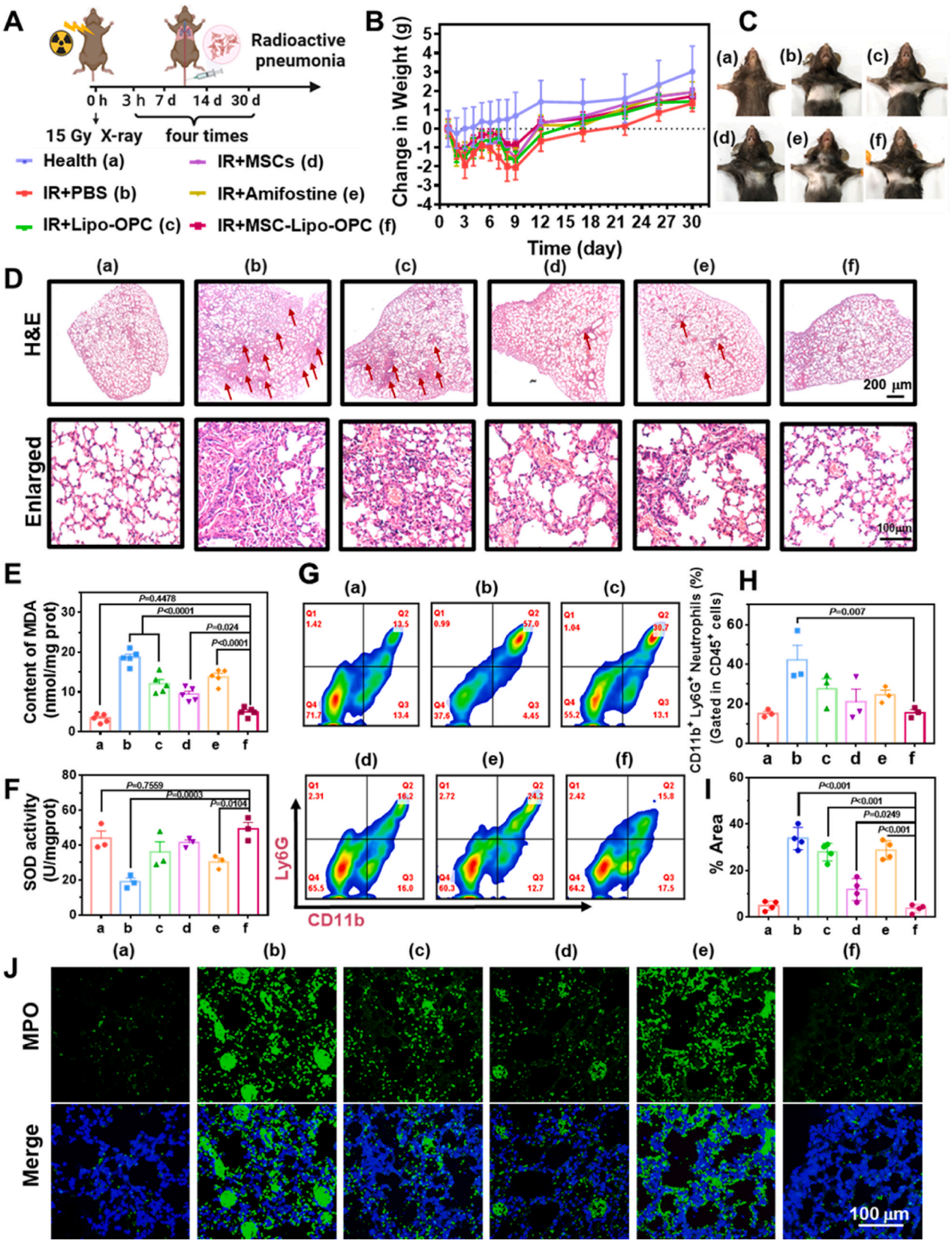

Fig. 5. ROS clearance by MSC-Lipo-OPC in mice with RILI. (A) Schematic diagram of treatment options for acute radiation pneumonia. (B) Changes in grams of body weight of mice in different treatment groups during 30 days. (C) The representative photographs of mice in different groups. (D) H&E staining images of lung tissue. (*E*–F) The MDA (E) and SOD (F) content of lung tissues collected from mice with various treatments. (G–H) Representative flow cytometry plots (G) and quantification (H) of neutrophil proportions in lung tissue suspensions collected from mice with the indicated treatments (n = 3). (I–J) Representative confocal image (J) and statistical data (I) of MPO expression in lung tissue sections collected from mice with indicated treatments (n = 4). Statistical significance was calculated via one-way analysis of variance (ANOVA).

macrophages are the main source of inflammatory cytokines) and F4/80^{hi}CD11b^{+} CD206^{+} repair macrophages (M2, M2 subtype macrophages can control the inflammatory response). The results showed that X-ray irradiation increased the activation and recruitment of M1 macrophages in the irradiated lung. MSC-Lipo-OPC could reduce the number of M1 macrophages and enhance the number of M2, which increased the repair of the injured site of the lung by secreting immunomodulatory factor and angiogenesis factor (Fig. 6A&B&D&E) [37,38]. At the same time, quantitative statistics were conducted on the number of CD4^{+} CD3^{+} Foxp3^{+} regulatory T cells (Tregs). The number of Tregs was increased after MSC-Lipo-OPC treatment, which was conducive to maintaining immune homeostasis (Fig. 6C&F). Tregs exhibited anti-inflammatory effects primarily through contact dependent inhibition of other immune cells, including CD4^{+} and CD8^{+} T cells, B cells, natural killer cells, and dendritic cells, as well as the release of cytokines, such as IL-10 and transforming growth factor [39].

Next, to determine whether MSC-Lipo-OPC had superior therapeutic properties in tissue recovery, we examined the expression levels of various angiogenic factors and inflammatory cytokines. Firstly, MSC-Lipo-OPC could decrease the X-ray-enhanced serum IFN-γ expression to normal level in healthy mice (Fig. S11). In addition, the expression trend of TNF−α was similar to that of IFN-γ (Fig. 6G). All treatments could reduce the level of TNF-α and MSC-Lipo-OPC treatment had the best effect. Notably, amifostine could not significantly reduce the IFN-γ and TNF-α expression, mainly owing to that amifostine could only reduce the ionizing radiation-associated free radicals, but have no therapeutic effect on concurrent inflammation or cytokine expression. These results indicated that MSC-Lipo-OPC was better than the early protective agent amifostine in the treatment of RILI by inhibiting the expression of cytokines in the inflammatory stage. The therapeutic efficacy of Lipo-OPC and amifostine was weaker than that of MSCs, probably on account of vascular damage/dysfunction in the weeks after X-ray irradiation [40]. Hepatocyte growth factor (HGF) is a multipotent growth factor that regulates tissue/vascular regeneration and damage repair, and vascular endothelial growth factor (VEGF) also promotes the growth of vascular endothelial cells and induces angiogenesis and reconstruction in vivo [41]. Then, we detected that MSC-Lipo-OPC could increase the contents of HGF and VEFG in the lung tissue of RILI mice. Compared with IR group, the expression of HGF and VEGF were increased by 10.02 times and 1.45 times in IR + MSC-Lipo-OPC group (Fig. 6H&I). Moreover, compared with other treatments, MSC-Lipo-OPC significantly increased the expression of the cytoskeletal protein vimentin, suggesting that MSC-Lipo-OPC could maintain the normalcy of injured Type II Alveolar Epithelial Cells (AEC II) (Fig. 6J&S12).

3.6. MSC-Lipo-OPC for relieving radiation pulmonary fibrosis

The persistent radiation pneumonia would eventually lead to the appearance of pulmonary fibrosis, resulting in the deterioration of lung function even the death. To investigate the antifibrotic efficacy of MSC-Lipo-OPC in RILI, we prolonged the inspection time to 6 months after radiation (Fig. 7A). Except for the MSC-Lipo-OPC-treated mice, the weight of mice in other groups was difficult to recover to the standard level of the weight of normal mice. After four months, mice in IR + PBS and IR + Lipo-OPC groups were gradually emasculated and lost significant weight, and therefore the mortality was also significantly increased (Fig. 7B). Meanwhile, oxyhemoglobin saturation decreased to about 90.12% ± 4.95% in the IR + PBS group and could be significantly improved by MSC-Lipo-OPC treatment (Fig. 7C). The low level of oxyhemoglobin saturation could seriously affect the quality of life of patients even induce the death. More importantly, CT imaging scan showed that the substantial density of mice lung in IR + PBS group was increased and MSC-Lipo-OPC lowed the X-ray-enhanced lung density to the healthy level (Fig. 7D). The high-density shadow in CT images indicated the appearance of inflammation and even fibrosis. Then, the photographs of dissected lungs also showed lung ischemia and thickened lung surface texture caused by lung fibrosis. From the images, we found that X-ray induced severe substantial lung disease, while MSC-Lipo-OPC could prevent the occurrence of lung fibrosis (Fig. 7E). Furthermore, H&E and Masson staining were conducted to test the role of MSC-Lipo-OPC in the reduction of collagen I deposition and repair of lung tissue. In IR + PBS group, a plenty of alveolar structures were destroyed and the alveolar wall was significantly thickened. Moreover, we found the accumulation of collagen and the aggravation of alveolar heterogeneity in the H&E-staining image of X-ray-treated lung tissue. In contrast, MSC-Lipo-OPC could significantly reduce the collapsed part, narrow the alveolar space, and thin the alveolar walls, suggesting that MSC-Lipo-OPC had a greater repair effect on alveolar structure than other treatments (Fig. 7F). Masson staining further proved the anti-fibrosis therapeutic effect of MSC-Lipo-OPC. The lungs of mice in IR + PBS group had a large area of muscle fibers, thickened alveolar walls and blood vessel walls, and a large amount of collagen deposition was around blood vessels and bronchi (Fig. 7G&S13). The treatment of MSC-Lipo-OPC could maintain the morphology of alveolar and bronchial epithelial cells, and had a good effect on the prevention of radioactive pulmonary fibrosis. Finally, the expression of α-SMA, which is closely related to the severity of fibrosis, was checked in the lung tissue with the indicated treatments. As shown in Fig. S14, X-ray exposure increased the expression of α-SMA in the exposed lungs, which could not be attenuated by Lipo-OPC and amifostine. On the contrary, MSC-Lipo-OPC significantly decreased the radiation-enhanced α-SMA expression, indicating that this anti-oxidative liposome-anchored MSC prevented the progress of radiation-induced pulmonary fibrosis.

Taken together, Lipo-OPC was proven to effectively eliminate ROS and accelerate the proliferation of vascular endothelial cells at low concentration. After this nanoparticle was linked to the membrane surface of MSCs, the released OPC from nanoparticles could act in close proximity to both of the inflammatory tissue and MSCs. In this way, OPC in MSC-Lipo-OPC could directly participate in the anti-inflammatory response and regulate the anti-inflammatory ability of MSCs, resulting in a perfect anti-inflammatory ability of MSC-Lipo-OPC. Besides, MSCs, which can be targeted to the damage site owing to their inflammatory tendency, could carry a plenty of OPC to the RILI site, improving the targeted delivery of OPC. Therefore, our obtained MSC-Lipo-OPC overcame the respective shortcomings of MSCs and antioxidant OPC, and showed an ideal efficacy for relieving radiation pneumonia/fibrosis.

4. Conclusion

In summary, we firstly obtained OPC-loaded liposome and verified its antioxidant. Furthermore, this liposome (Lipo-OPC) could be modified with DSPE-PEG-DBCO during preparation and further attached to the membrane surface of Ac4ManNAz-treated MSCs via click chemical reaction, yielding drug-anchored MSC (MSC-Lipo-OPC). Notably, the drug loading process did not affect the viability, inflammatory tendency and proangiogenic properties of MSCs. Upon intravenous injection, MSC-Lipo-OPC targeted to the X-ray-exposed lungs and retained in the lesion location for a long time owing to the micron size and inflammatory targeting properties of MSCs. Additionally, the X-ray-triggered ROS production could be significantly reduced by MSC-Lipo-OPC, resulting in the limited acute radiation pneumonia. Moreover, MSC-Lipo-OPC injection leaded to the reduced infiltration of neutrophils, which is the main cell that produces ROS during inflammation. Besides, the macrophages in lung lesions tended to be polarized towards M2 and the quantity of Tregs increased after MSC-Lipo-OPC treatment. These two kinds of innate-immune-cells and their secreted cytokines could further promote anti-inflammatory and tissue repair. Finally, MSC-Lipo-OPC treatment could also significantly improve the lung function of X-ray-treated mice and slow down the progression of radioactive fibrosis in the later stages of radiation lung injury. Therefore, the drug-anchored MSCs we designed could synergistically exert the anti-inflammatory effects of drugs and MSC, providing an effective treatment strategy for radiation pneumonia/fibrosis.

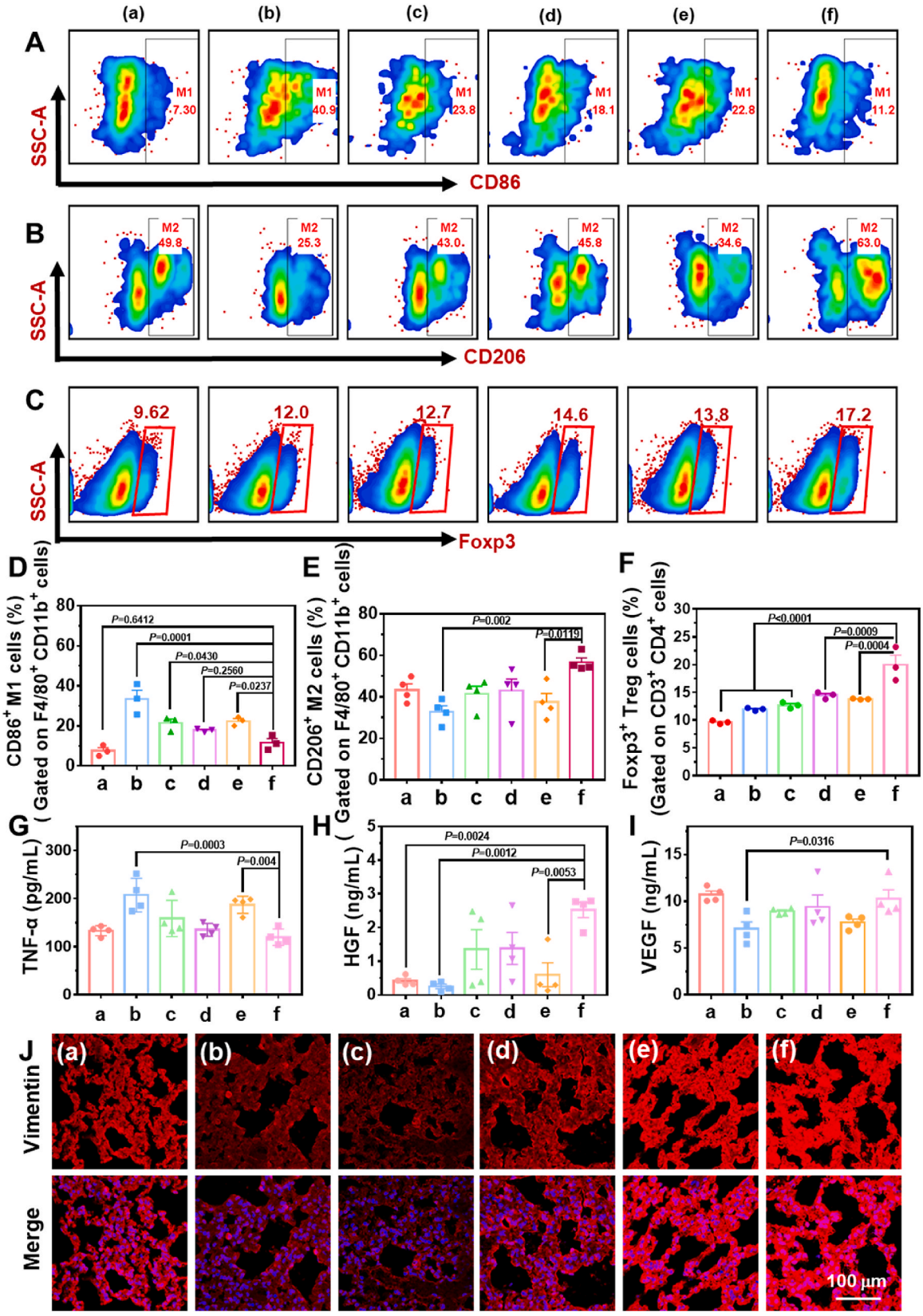

Fig. 6. The proportion analysis of anti-inflammatory innate immune cells and the evaluation of tissue repair level. (A–C) Representative flow cytometry plots of M1 macrophages (A), M2 macrophages (B) and Treg cells (C) in lung tissues of each group. (D–F) Quantification of the proportion of M1 macrophages (D), M2 macrophages (E) and Treg cells (F) in A-C. (G–I) Quantification of cytokines, including TNF-α. (G), HGF (H) and VEGF (I), in serum collected from mice in each group. (J) Immunofluorescence images of vimentin (red) in lung tissue of each group at 33 days after X-ray irradiation (scale bar: 100 μm). Statistical significance was calculated via one-way analysis of variance (ANOVA).

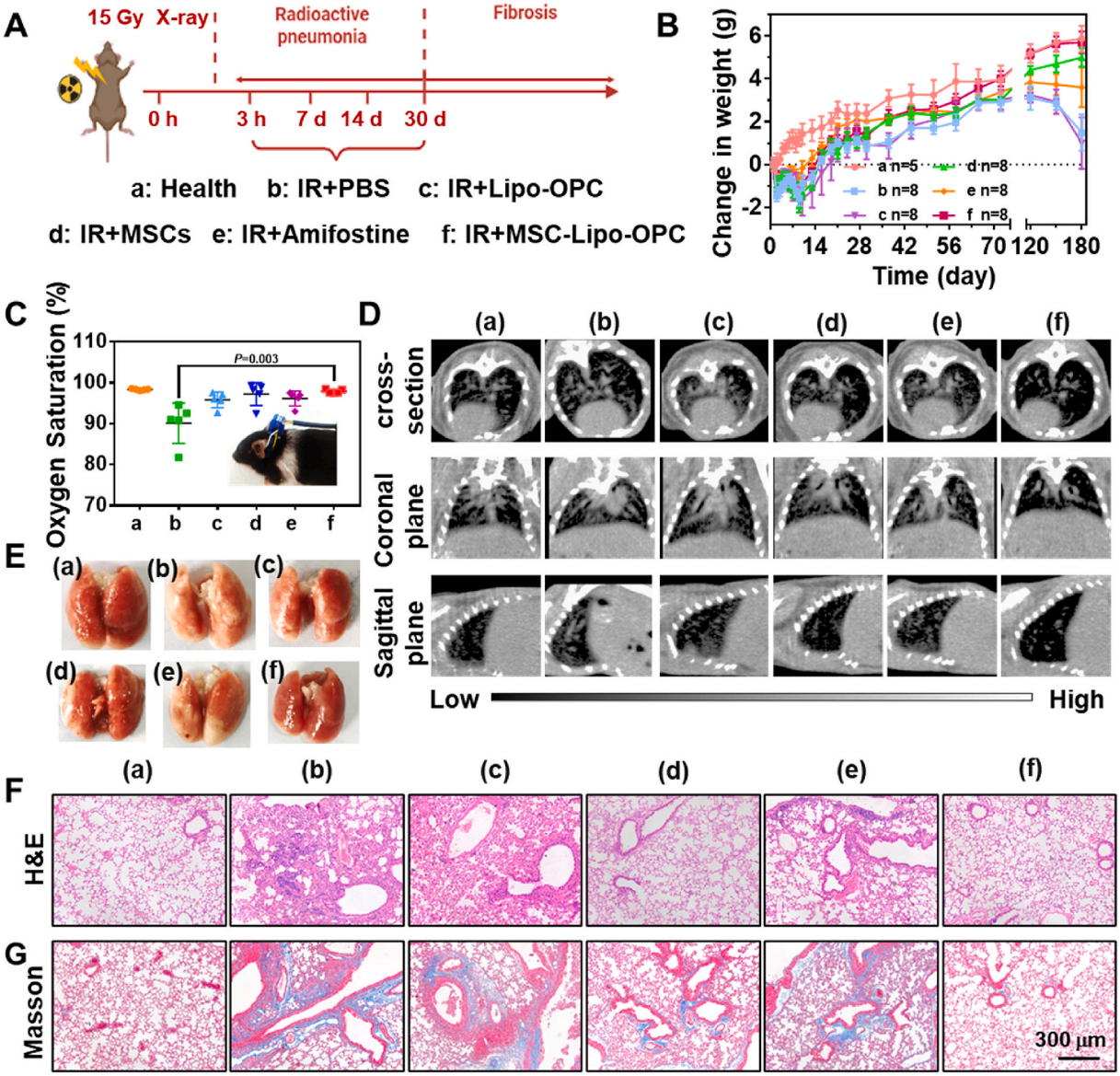

Fig. 7. The effect of MSC-Lipo-OPC on the radiation-induced pulmonary fibrosis. (A) Schematic representation of the treatment regimen. (B) The body weight of mice with indicated treatment in 180 days. (C) The oxygen saturation of mice in each group (n = 5). (D) CT imaging of the chest of mice in each group in cross-section, coronal plane and sagittal plane. (E) The representative photographs of whole lungs collected from mice with indicated treatment. (F–G) H&E staining (F) and Masson staining (G) of lung section collected from mice with indicated treatment (scale bar: 300 μm). Statistical significance was calculated via one-way analysis of variance (ANOVA).

Credit author statement

Y. K., X.Y. and H.Z. conceived the project; H.Z. carried out the synthesis of MSC-Lipo-OPC and detected the therapeutic effect of MSC-Lipo-OPC on radiation pneumonia/fibrosis in vitro and in vivo; Y.Z. assisted to build mouse models of RILI; P.P. and W.S. performed flow cytometry of immune cells; Y. K., X.Y., and H.Z. wrote the manuscript.

Declaration of competing interest

The authors declare that they have no known competing financial interests or personal relationships that could have appeared to influence the work reported in this paper.

Data availability

Data will be made available on request.

Acknowledgements

This work was partially supported by the National Natural Science Foundation of China (U1932208, 32171382, U2032134, 31900986), Key Research and Development Program of Social Development of Jiangsu Province (BE2022725), and the Project Funded by the Priority Academic Program Development of Jiangsu Higher Education Institutions (PAPD).

Appendix A. Supplementary data

Supplementary data to this article can be found online at https://doi.org/10.1016/j.biomaterials.2023.122202.

References

[1] A.N. Hanania, W. Mainwaring, Y.T. Ghebre, N.A. Hanania, M. Ludwig, Radiation-induced lung injury: assessment and management, Chest 156 (1) (2019) 150–162.

[2] S. Drishya, S.S. Dhanisha, P. Raghukumar, C. Guruvayoorappan, Amomum subulatum mitigates experimental thoracic radiation-induced lung injury by regulating antioxidant status and inflammatory responses, Food Funct. 14 (3) (2023) 1545–1559.

[3] S.P. Newman, Delivering drugs to the lungs: the history of repurposing in the treatment of respiratory diseases, Adv. Drug Deliv. Rev. 133 (2018) 5–18.

[4] D. Kauffmann-Guerrero, J. Taugner, C. Eze, L. Käsmann, M. Li, A. Tufman, F. Manapov, Clinical management and outcome of grade III pneumonitis after chemoradioimmunotherapy for inoperable stage III non-small cell lung cancer-A prospective longitudinal assessment, Diagnostics 11 (11) (2021) 1968.

[5] L. Käsmann, A. Dietrich, C.A. Staab-Weijnitz, F. Manapov, J. Behr, A. Rimner, B. Jeremic, S. Senan, D. De Ruysscher, K. Lauber, C. Belka, Radiation-induced lung toxicity - cellular and molecular mechanisms of pathogenesis, management, and literature review, Radiat. Oncol. 15 (1) (2020) 214.

[6] J. Xie, C. Wang, F. Zhao, Z. Gu, Y. Zhao, Application of multifunctional nanomaterials in radioprotection of healthy tissues, Advanced healthcare materials 7 (20) (2018). Article e1800421.

[7] T. Liu, Q. Yang, H. Zheng, H. Jia, Y. He, X. Zhang, J. Zheng, Y. Xi, H. Zhang, R. Sun, X. Chen, W. Shan, Multifaceted roles of a bioengineered nanoreactor in repressing radiation-induced lung injury, Biomaterials 277 (2021). Article 121103.

[8] M. Luo, L. Chen, J. Zheng, Q. Wang, Y. Huang, F. Liao, Z. Jiang, C. Zhang, G. Shen, J. Wu, Y. Wang, Y. Wang, Y. Leng, S. Han, A. Zhang, Z. Wang, C. Shi, Mitigation of radiation-induced pulmonary fibrosis by small-molecule dye IR-780, Free Radic. Biol. Med. 164 (2021) 417–428.

[9] X. Chang, L. Xing, Y. Wang, C.X. Yang, Y.J. He, T.J. Zhou, X.D. Gao, L. Li, H.P. Hao, H.L. Jiang, Monocyte-derived multipotent cell delivered programmed therapeutics to reverse idiopathic pulmonary fibrosis, Sci. Adv. 6 (22) (2020). Article eaba3167.

[10] S. Azarmi, W.H. Roa, R. Löbenberg, Targeted delivery of nanoparticles for the treatment of lung diseases, Adv. Drug Deliv. Rev. 60 (8) (2008) 863–875.

[11] J. Galipeau, L. Sensébé, Mesenchymal stromal cells: clinical challenges and therapeutic opportunities, Cell Stem Cell 22 (6) (2018) 824–833.

[12] Y. Yan, J. Fu, R.O. Kowalchuk, C.M. Wright, R. Zhang, X. Li, Y. Xu, Exploration of radiation-induced lung injury, from mechanism to treatment: a narrative review, Transl. Lung Cancer Res. 11 (2) (2022) 307–322.

[13] L.M. Abernathy, M.D. Fountain, S.E. Rothstein, J.M. David, C.K. Yunker, J. Rakowski, F. Lonardo, M.C. Joiner, G.G. Hillman, Soy isoflavones promote radioprotection of normal lung tissue by inhibition of radiation-induced activation of macrophages and neutrophils, J. Thorac. Oncol. : official publication of the International Association for the Study of Lung Cancer 10 (12) (2015) 1703–1712.

[14] L. Meziani, M. Mondini, B. Petit, A. Boissonnas, V. Thomas de Montpreville, O. Mercier, M.C. Vozenin, E. Deutsch, CSF1R inhibition prevents radiation pulmonary fibrosis by depletion of interstitial macrophages, Eur. Respir. J. 51 (3) (2018). Article 1702120.

[15] O. Levy, R. Kuai, E.M.J. Siren, D. Bhere, Y. Milton, N. Nissar, M. De Biasio, M. Heinelt, B. Reeve, R. Abdi, M. Alturki, M. Fallatah, A. Almalik, A.H. Alhasan, K. Shah, J.M. Karp, Shattering barriers toward clinically meaningful MSC therapies, Sci. Adv. 6 (30) (2020). Article eaba6884.

[16] E.A. Kimbrel, R. Lanza, Next-generation stem cells - ushering in a new era of cell-based therapies, Nat. Rev. Drug Discov. 19 (7) (2020) 463–479.

[17] J. Wang, Z. Cao, P. Wang, X. Zhang, J. Tang, Y. He, Z. Huang, X. Mao, S. Shi, X. Kou, Apoptotic extracellular vesicles ameliorate multiple myeloma by restoring fas-mediated apoptosis, ACS Nano 15 (9) (2021) 14360–14372.

[18] I. Fernández-Ruiz, Boosting stem cell vascular regenerative capacity, Nat. Rev. Cardiol. 18 (5) (2021) 306.

[19] X. Xia, K.F. Chan, G.T.Y. Wong, P. Wang, L. Liu, B.P.M. Yeung, E.K.W. Ng, J.Y. W. Lau, P.W.Y. Chiu, Mesenchymal stem cells promote healing of nonsteroidal anti-inflammatory drug-related peptic ulcer through paracrine actions in pigs, Sci. Transl. Med. 11 (516) (2019). Article eaat7455.

[20] S. Lim, H.Y. Yoon, H.J. Jang, S. Song, W. Kim, J. Park, K.E. Lee, S. Jeon, S. Lee, D. K. Lim, B.S. Kim, D.E. Kim, K. Kim, Dual-modal imaging-guided precise tracking of bioorthogonally labeled mesenchymal stem cells in mouse brain stroke, ACS Nano 13 (10) (2019) 10991–11007.

[21] T. Lan, M. Luo, X. Wei, Mesenchymal stem/stromal cells in cancer therapy, J. Hematol. Oncol. 14 (1) (2021) 195.

[22] J. Han, Y. Liu, H. Liu, Y. Li, Genetically modified mesenchymal stem cell therapy for acute respiratory distress syndrome, Stem Cell Res. Ther. 10 (1) (2019) 386.

[23] N.N. Ng, A.S. Thakor, Locoregional delivery of stem cell-based therapies, Sci. Transl. Med. 12 (547) (2020). Article eaba4564.

[24] J.M. Karp, G.S. Leng Teo, Mesenchymal stem cell homing: the devil is in the details, Cell Stem Cell 4 (3) (2009) 206–216.

[25] M. Hao, S. Hou, W. Li, K. Li, L. Xue, Q. Hu, L. Zhu, Y. Chen, H. Sun, C. Ju, C. Zhang, Combination of metabolic intervention and T cell therapy enhances solid tumor immunotherapy, Sci. Transl. Med. 12 (571) (2020). Article eaaz6667.

[26] M. Gutmann, J. Bechold, J. Seibel, L. Meinel, T. Lühmann, Metabolic glycoengineering of cell-derived matrices and cell surfaces: a combination of key principles and step-by-step procedures, ACS Biomater. Sci. Eng. 5 (1) (2019) 215–233.

[27] X. Kou, X. Xu, C. Chen, M.L. Sanmillan, T. Cai, Y. Zhou, C. Giraudo, A. Le, S. Shi, The Fas/Fap-1/Cav-1 complex regulates IL-1RA secretion in mesenchymal stem cells to accelerate wound healing, Sci. Transl. Med. 10 (432) (2018). Article eaai8524.

[28] J.M. Lv, M. Gouda, X.Q. Ye, Z.P. Shao, J.C. Chen, Evaluation of proanthocyanidins from kiwi leaves (actinidia chinensis) against caco-2 cells oxidative stress through nrf2-ARE signaling pathway, Antioxidants 11 (7) (2022) 1367.

[29] Y. Yang, Y. Zhao, R. Lai, L. Xian, Q. Lei, J. Xu, M. Guo, D. Xian, J. Zhong, An emerging role of proanthocyanidins on psoriasis: evidence from a psoriasis-like mouse model, Oxid. Med. Cell. Longev. 2022 (2022). Article 5800586.

[30] H. Wang, P. Lu, Z. Li, C. Yuan, H. Liu, J. Zhao, W. Lu, J. Wang, Oligomeric proanthocyanidins and bamboo leaf flavonoids improve the quality of bull semen cryopreservation, Molecules 27 (3) (2022) 1144.

[31] F.C. Liu, H.P. Yu, P.J. Chen, H.W. Yang, S.H. Chang, C.C. Tzeng, W.J. Cheng, Y. R. Chen, Y.L. Chen, T.L. Hwang, A novel NOX2 inhibitor attenuates human neutrophil oxidative stress and ameliorates inflammatory arthritis in mice, Redox Biol. 26 (2019). Article 101273.

[32] T. Sun, Q. Chen, Z. Zhou, C. Li, T. Yu, C. Jiang, A chemiluminescent reporter assisted by in-situ neutrophils for imaging O_2 at inflammatory sites, J. Contr. Release 358 (2023) 382–397.

[33] X. Zhang, J. Tang, X. Kou, W. Huang, Y. Zhu, Y. Jiang, K. Yang, C. Li, M. Hao, Y. Qu, L. Ma, C. Chen, S. Shi, Y. Zhou, Proteomic analysis of MSC-derived apoptotic vesicles identifies Fas inheritance to ameliorate haemophilia a via activating platelet functions, J. Extracell. Vesicles 11 (7) (2022). Article e12240.

[34] J. Du, M.A. Meledeo, Z. Wang, H.S. Khanna, V.D. Paruchuri, K.J. Yarema, Metabolic glycoengineering: sialic acid and beyond, Glycobiology 19 (12) (2009) 1382–1401.

[35] K.S. Kim, J.Y. Lee, J. Han, H.S. Hwang, J. Lee, K. Na, Local immune-triggered surface-modified, Stem Cells for Solid Tumor Immunotherapy 29 (26) (2019). Article 1900773.

[36] J. Liu, F. Hu, M. Wu, L. Tian, F. Gong, X. Zhong, M. Chen, Z. Liu, B. Liu, Bioorthogonal coordination polymer nanoparticles with aggregation-induced emission for deep tumor-penetrating radio- and radiodynamic therapy, Adv. Mater. 33 (9) (2021). Article e2007888.

[37] J. Zhao, X. Li, J. Hu, F. Chen, S. Qiao, X. Sun, L. Gao, J. Xie, B. Xu, Mesenchymal stromal cell-derived exosomes attenuate myocardial ischaemia-reperfusion injury through miR-182-regulated macrophage polarization, Cardiovasc. Res. 115 (7) (2019) 1205–1216.

[38] T. Chen, Q. Cao, Y. Wang, D.C.H. Harris, M2 macrophages in kidney disease: biology, therapies, and perspectives, Kidney Int. 95 (4) (2019) 760–773.

[39] L. So, K. Obata-Ninomiya, A. Hu, V.S. Muir, A. Takamori, J. Song, J.H. Buckner, R. Savan, S.F. Ziegler, Regulatory T cells suppress $CD4^+$ effector T cell activation by controlling protein synthesis, J. Exp. Med. 220 (3) (2023). Article e20221676.

[40] M.O. Lee, S.H. Song, S. Jung, S. Hur, T. Asahara, H. Kim, S.M. Kwon, H.J. Cha, Effect of ionizing radiation induced damage of endothelial progenitor cells in vascular regeneration, Arterioscler. Thromb. Vasc. Biol. 32 (2) (2012) 343–352.

[41] Z. Cao, T. Ye, Y. Sun, G. Ji, K. Shido, Y. Chen, L. Luo, F. Na, X. Li, Z. Huang, J.L. Ko, V. Mittal, L. Qiao, C. Chen, F.J. Martinez, S. Rafii, B.S. Ding, Targeting the vascular and perivascular niches as a regenerative therapy for lung and liver fibrosis, Sci. Transl. Med. 9 (405) (2017). Article eaai8710.